

Contents lists available at ScienceDirect

Materialia

journal homepage: www.elsevier.com/locate/mtla



Full Length Article

Enhancing mechanical properties of Electrospun Cellulose Acetate Fiber Mat upon Potassium Chloride exposure



Ruhit Sinha^a, Srinivas Janaswamy^b, Anamika Prasad^{a,*}

- ^a Mechanical Engineering, South Dakota State University, Brookings, SD, 57007, U.S.A.
- ^b Dairy and Food Science, South Dakota State University, Brookings, SD, 57007, U.S.A.

ARTICLE INFO

Keywords: Electrospinning Cellulose acetate Potassium Chloride Tensile Strength Mechanical Properties Bone Tissue Engineering

ABSTRACT

Cellulose acetate (CA) based biomaterials are being used as substrates for bone ingrowth applications due to their non-toxic and non-irritant nature coupled with optimum morphology and stiffness. Electrospinning with additives and/or post-treatment has emerged as a viable protocol to improve the mechanical properties of CA further and expand its utility. Herein, we highlight the role of potassium chloride (KCl) in association with air-drying to enhance the elastic modulus and tensile strengths of CA fiber mats. Salt aggregation between fibers was observed through Scanning Electron Microscopy (SEM). However, Fourier-transform infrared (FTIR) analysis indicates the interactions between K+ ions and acetyl groups. X-ray diffraction (XRD) study suggests the retention of CA structure in the CA-KCl mats and the excess presence of KCl. The increase in KCl concentration (from 2 to 6%) boosts the elastic modulus to 176 MPa (52 times than pure CA) and tensile strength to 1.2 MPa (9 times than pure CA). Indeed, the presence of K+ ions offers osteoconduction to fiber mats, and thus the outcome has potential in bone tissue engineering.

1. Introduction

Cellulose is the most abundant organic compound found on earth. It has the highest stiffness to density ratio among other natural materials [1]. It also has the multifunctionality of fibrous structure, excellent biocompatibility, and high water absorbance [2,3]. Consequently, cellulose and cellulose-based polymers have been investigated for a host of applications, including water filtration, food delivery, and tissue engineering scaffold [4–10]. However, pure cellulose is water-insoluble, requiring the use of harsh chemicals during manufacturing [3,11]. Consequently, cellulose derivatives such as Cellulose acetate (CA) find use as cellulose alternative with similar advantages in terms of mechanical properties, biocompatibility, and degradability. Cellulose acetate (CA) based scaffolds have found widespread use in biomedical applications such as for bone [12–14], cartilage [15], skin [16], and neural tissue regeneration [17].

For tissue engineering applications, replicating a fibrous scaffold structure similar to the extracellular matrix of native tissue is critical to support cell function for tissue regeneration. Towards this end, electrospinning has emerged as a viable, cost-effective, and successful manufacturing tool to engineer submicron to nanoscale fibers for tissue engineering and other applications requiring fibrous

structure such as in air filtrations [18–24]. The morphology of the electrospun fibers can be fine-tuned to meet application-specific requirements by controlling the electrospinning parameters, namely voltage, types of collectors, solvent(s), solution concentration, flow rate, and tip-to-collector distance [25]. From the above parameters, solvent plays a critical role in producing uniform, ultrafine and defect-free fibers. Importantly, solvents such as acetone with lower surface tension leading to high dispersion force are favored [26]. For example, with acetone solvent, bead-free CA fibers of 1 μ m diameter were produced [27].

Other solvents or combinations of solvents have also been used in CA fiber formation, as listed in Table 2. Significant variability in fiber strength and geometry have been reported, with elastic modulus varying from 1 MPa to 400 MPa, tensile strength from 1.2 MPa to 49 MPa [24,28–32], and fiber diameter from 35 nm to 65,000 nm [26]. The observed variations are due to differences in electrospinning parameters and strain rate of the tensile test (Table 2). Tests conducted at a higher strain rate exhibit increased stiffness and strength than those performed at lower strain rates [33]. Overall, pure CA fibers are fluffy and have inadequate mechanical strengths for most applications. Thus, modifications are warranted to enhance mechanical properties, e.g., through additives and/or post-treatment.

E-mail address: Anamika.Prasad@sdstate.edu (A. Prasad).

^{*} Corresponding author.

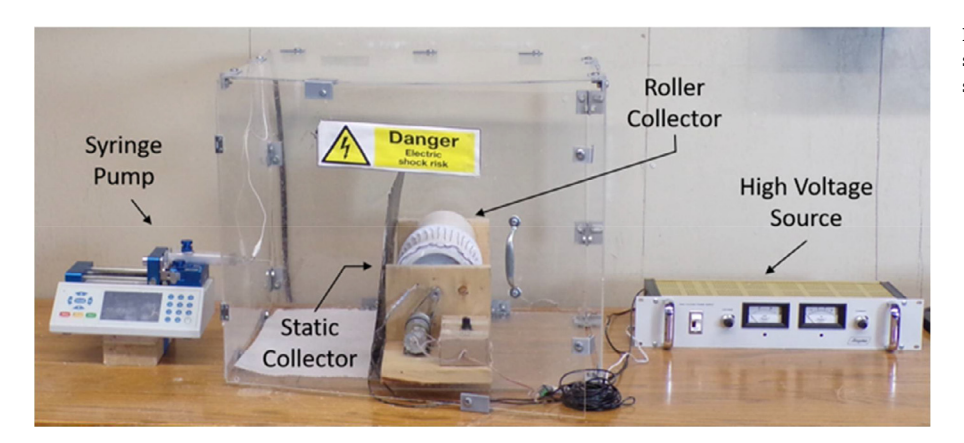


Fig. 1. The in-house electrospinning setup used in the study with the major components marked. We used the static collector plate for the study.

Several studies have evaluated such modifications for CA-based fiber formation. For instance, heat treatment at 208°C for 1 h augments tensile strength to 5 MPa from the initial 1.2 MPa [28]. The fusion of fibers just above the glass-transition temperature appears to be responsible for the observed increase. Similarly, deacetylation with Na2CO3 followed by washing resulted in 2.5 times increased in tensile strength from 2.16 to 5.24 MPa due to its conversion to pure cellulose, enabling newly formed hydroxyl groups holding the chains tighter via hydrogen bonds [29]. Modifications involving certain additives and fillers led to even more remarkable changes in the mechanical properties. For example, the presence of 0.5 wt% carbon nanotube elevates the tensile strength by about 3 times: 40 to 135 MPa and Young's modulus by about 11 times: 100 to 1100 MPa [30]. Similarly, graphene and graphene-COOH upsurge Young's modulus to 910 MPa from the initial 245 MPa (pure CA) [24]. In another study, the CA-Graphene oxide composite demonstrated Young's modulus from 400 MPa to 1600 MPa and tensile strength from 49 MPa to 97.5 MPa compared to pure CA values [31].

Another approach of strengthening CA material is by use of natural fillers such as collagen and chitosan. The CA matrix impregnation with these biopolymers as fillers to form sponge-woven scaffolds results with a tensile strength of 40 MPa and Young's modulus of 600 MPa compared to pure CA values 3.8 MPa and 34.7 MPa respectively [32]. In another study, Chitosan/cellulose acetate nanofibers fabricated through electrospinning demonstrated higher tensile strength of 17 MPa compared to 2.2 MPa of pure CA [29].

The examples stated above suggest the seminal role of additives on improving the mechanical properties of CA fibers. The choice of additives or post-processing also depends on targeted applications. Additives that potentially show bioactivity to enhance tissue regeneration and osteointegration will be preferred for bone tissue applications. It has been demonstrated in an ex-vivo cell-culture experiment that potassium ions (K⁺) release from the alkaline treated calcium phosphate coating of Ti-24Nb-4ZR-7.6Sn alloy can promote osteoblast adhesion and proliferation [34]. A similar in-vitro study of human alveolar bone cell culture on ion-implanted titanium found the influence of ${}^{40}\text{Ca}^{+}$ and ${}^{39}\text{K}^{+}$ ions on the surface chemistry enhancing the osseointegration [35]. These studies point towards the benefit of K⁺ ions in bone tissue regeneration. In the context of cellulose, inorganic non-aggressive solvents, including potassium chloride (KCl) solution in water, have been used for cellulose solubilization and mechanical property modulation by chemically interacting with cellulose polymer backbone [36].

Hence, the above leads us to hypothesize that the KCl solution can modulate the mechanical properties of electrospun CA fibers, which can have potential promising applications for bone tissue engineering. Towards the end, here we investigate the interactions and strengthening influences of K⁺ ions on electrospun CA fibers by treating with varying concentrations of KCl (CA-KCl fibers). The structure and response of native and processed CA-KCl fibers are analyzed using multiple experimental techniques to identify the underlying mechanisms.

2. Materials and methods

2.1. Materials

CA with average molecular weight 30,000 g/mol and degree of acetylation 39.8% was purchased from Sigma Aldrich. Acetone of HPLC Grade was purchased from EMD Millipore. KCl was purchased from VWR. All the chemicals were used as received without further purification.

2.2. Electrospinning

Cellulose-based fiber mats were prepared using an in-house built electrospinning platform consisting of a 20 mL syringe with a 14-gauge spinneret and Chemyx Fusion 100 pump, a rack Mounting Linear regulated power supply (Acopian), and arrangement with static and roller collector. Fig. 1 shows the setup with the components marked.

A solution of 15 wt% cellulose acetate was dissolved in acetone using hot plate and magnetic stirrer at 150 rpm and 22°C for around 20 min until a homogenous solution was achieved. Since higher concentration contributed to increased viscosity [26,27], a 15 wt% solution was viscous enough to form bead-free fibers. The electrospinning parameters included a flow rate of 0.2 mL/min, an applied voltage of 15 kV, and a static horizontal collector made of aluminum foil with dimension 35 cm x 15 cm at around 18 cm from the spinneret. The electrospinning was performed for approximately 125 min at room temperature and average humidity. The volatile nature of acetone enabled easy peeling of the fiber mat from the foil. However, the spinneret needs to be cleaned regularly due to clogging to maintain the uniformity of fiber generation.

2.3. Sample preparation

The fiber mats formed on the collector were peeled off gently, folded three times, and kept under weight overnight to flatten. The total thickness of the folded mat was found to be around 3 mm. The middle portion with dimension 16×2 cm was cut out to form a testing sample, as shown in Fig. 2b. A set of ten samples were tested as such with no further post-treatment. Other samples were post-treated by dipping in KCl-water solution of varying concentrations (2%, 4%, and 6%) and then air-dried overnight at room temperature (RT). Dipping in the solution can have other side effects such as pore removal to affect mechanical strength. Hence to study the effect of dipping, another set of three samples without KCl treatment was dipped in distilled water and air-dried at room temperature. The dipping and post drying resulted in shrinkage of the mat to a thickness of approximately 2 mm. Treatment with KCl as above was repeated with two other batches to dry at different temperatures inside an incubator: 37°C (Panasonic CellIQ CO2 Incubator) and 65°C (Blue M 100A Dry Type Bacteriological).

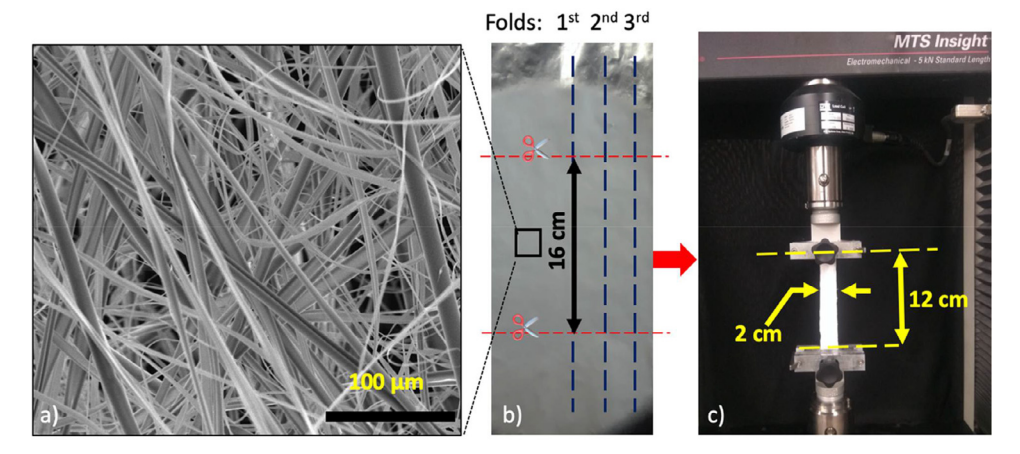


Fig. 2. a) SEM image of pure CA fiber mat; b) Folding of the fiber mat to form a testing sample of size $16 \text{ cm } \times 2 \text{ cm}$; and c) Tensile test setup with fabric clamp and a gauge length of the sample = 12 cm

2.4. Characterization

The weight of the post-processed fiber mats was measured, and a relative total weight for each set of mats was reported. Several tests were carried out for mechanical strength evaluation and fiber mat characterization, as indicated in Figs. 2a to 2c. Scanning electron microscopy (SEM) was used for fiber morphology of electrospun mat. The tensile test was used for mechanical property analysis. To understand the nature of the interaction of CA-KCl, FTIR and X-ray diffraction (XRD) analysis were also performed.

SEM was performed using Hitachi S-3400N. Prior to the observation, a piece of 5mm x 5mm fiber mat was cut out with scissors and placed in the specimen holder. They were sputter-coated using a CRC sputtering device with gold to minimize the electrostatic charge build-up on the non-conductive surface. The Au layer was 10 nm thick layer suitable for improving the quality of the high-resolution secondary-electron signal and preventing thermal damage [37]. The deposition was done at the rate of 0.2 $\rm \mathring{A}s^{-1}$ and the current setting of 35 mA on a 2 inch diameter, 0.125 inch thick target from Kurt J Lesker Co. The surfaces were observed at 10 kV.

The uniaxial tensile test was performed using Insight 4 (MTS Electromechanical Testing Systems) equipped with a 5 kN load cell. These tests were carried at a strain rate of 2 mm/min with a data acquisition rate of 50 Hz. The load versus deformation data was obtained directly without using an external strain gauge or digital image-correlation method. Mechanical properties such as elastic modulus, tensile strength, and percentage strain at failure were determined and reported. Further, mean and standard deviation values were calculated, and significant differences using the t-test were established wherever necessary.

FTIR was performed using Perkin Elmer Spectrum 65 FT-IR Spectrometer. XRD was performed using the Rigaku MiniFlex600 diffractometer operated at 35 kV and 15 mA. For XRD, the Cu $\rm K_{\alpha}$ radiation (l = 1.5406 Å) was used, and intensity data were collected in the angular range of 5 < 2 θ < 50° at a step size of 0.02° with the scan rate of 2° per min.

3. Results

3.1. Relative weight and Fiber morphology

The relative weight of the CA-KCl fiber mats was measured and reported in Fig. 3. It was observed that the relative weight increased as the concentration of KCl increased for all three drying temperatures, indicating a rise of salt deposition on the surfaces of fiber mats. The slope becomes smaller with an increase in drying temperatures to 37°C and 65°C. The above potentially indicates higher total evaporation of moisture trapped within the fibers at a higher temperature.

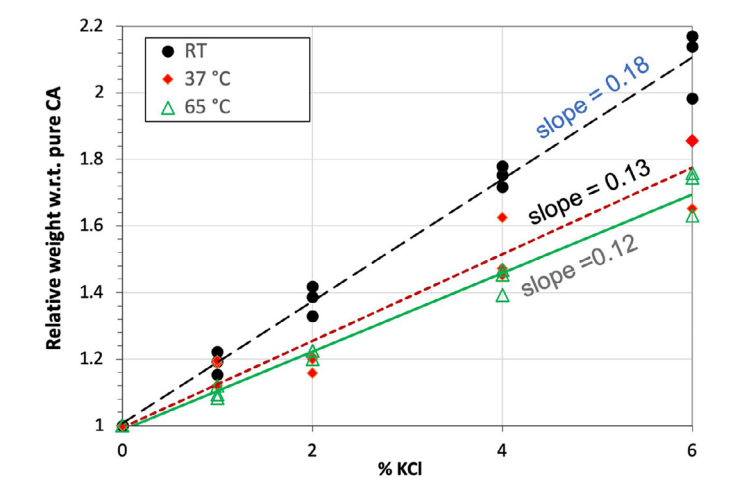


Fig. 3. Relative weight of CA-KCl fiber mats dried at RT, 37°C and 65°C. Number of samples = 3 for each type of fiber mats. Increasing temperature showed a decreasing trend in relative weight due to higher evaporation of trapped water.

A closer look at the morphology of CA-KCl fibers using SEM revealed clusters of salt deposits randomly on the fiber mat, physically bridging the intersecting fibers (Fig. 4). The salt deposition increased with the KCl concentration. Also, fewer clusters were observed at higher drying temperatures, probably due to greater dispersion of the KCl solution. It is to be noted that no fusion of CA due to melting can take place since the maximum temperatures used here of 65°C was much lower than the glass transition temperature (T_g) of 198–205°C, and melting temperature (T_m) of 224–230°C for CA [28].

3.2. FTIR Spectral Study

FTIR was conducted on pure CA and CA-KCl fiber mats to determine the nature of the interactions between CA fibers and KCl. The absorption bands were identified [38] and reported in Table 1.

Fig. 5a shows four representative FTIR plots for each fiber mat type with offset %Transmittance value on the y-axis for better comparison. All the peaks had nearly similar corresponding wavenumber except peak 2 attributed to C-O stretching of the acetyl group. Fig. 5b shows a closer view of the overlap of all four types of fiber mats at peak 2. It revealed a deviation of around 10 cm⁻¹, which is consistent and notable enough [24] to indicate a potential chemical interaction between the C-O bond in the acetyl group with the positively charged K⁺ ions.

Fig. 5c provides additional information about this interaction for peak 2. The lines show the average results of three samples at each temperature. A shift in peak location was observed at all temperatures

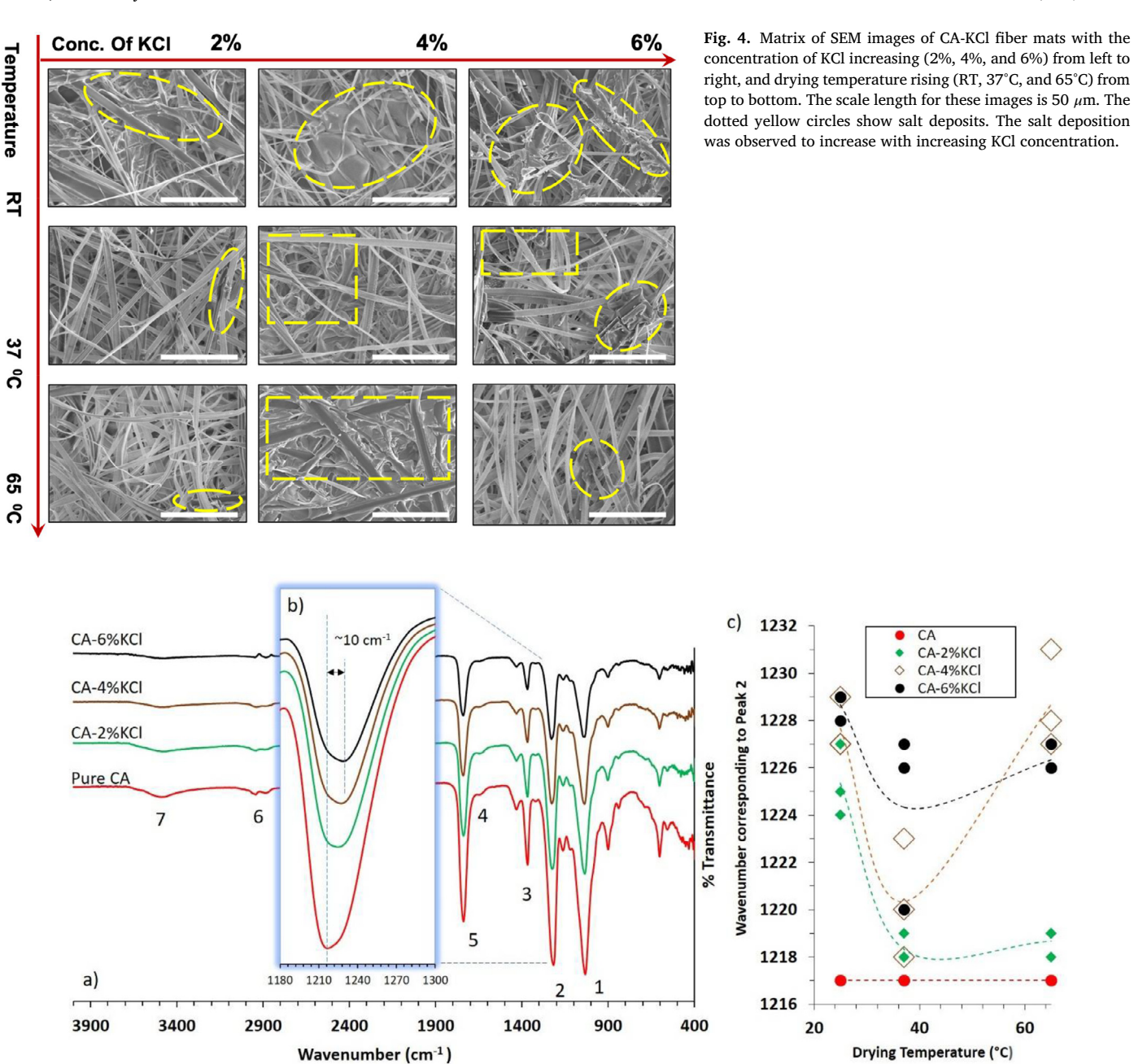


Fig. 5. a) The FTIR-spectra of all four types of fiber mats air-dried at room temperature; b) magnified view of the FTIR-spectra showing a 10 cm⁻¹ deviation of wavenumber at peak 2 attributed to C-O stretching of the acetyl group; c) a scatter plot showing shift in wavenumber at peak 2 depending on different drying temperatures for all types of fiber mats.

Table 1 Characteristic peaks of pure CA [38].

Peak No.	Wavenumber (cm ^{−1})	Corresponding peak
1	1033	C-O-C of the cellulose backbone
2	1217	C-O stretching of the acetyl group
3	1367	C-H bending vibration of CH ₃ in the acetyl group
4	1646	H-O-H bending of absorbed water
5	1738	C=O stretching of the acetyl group
6	2900-2950	C-H stretching of CH ₂ or CH
7	3400-3500	-OH stretching of unacetylated cellulose

for CA-KCl fiber mats but not for pure CA. This observation further indicates chemical reaction within CA-KCl fiber mat. For room temperature and at 35°C, the peak shift followed the trend of increasing value with

increasing KCl concentration, with the shift getting narrower at 37° C. Interestingly, at 65° C, all other CA-KCl fiber mats behaved as before except CA-4%KCl, which showed a considerable shift upward surpassing the values for CA-6%KCl. The above indicates that 4% KCl concentration is most sensitive to temperature fluctuations. Overall, these variations observed for KCl treated samples but not in pure CA is an additional indication of chemical interaction between C-O bond and K⁺ ions.

3.3. XRD Study

A wide-angle X-ray diffraction analysis was carried out to understand the specific dispersion behavior of KCl into the CA fiber mats within its crystalline region. The peaks of pure KCl and CA were used as the reference. Pure CA demonstrates two peaks at the diffraction angles 12.5° and 21.7° that are typical for cellulose originating from the (110) and (200)

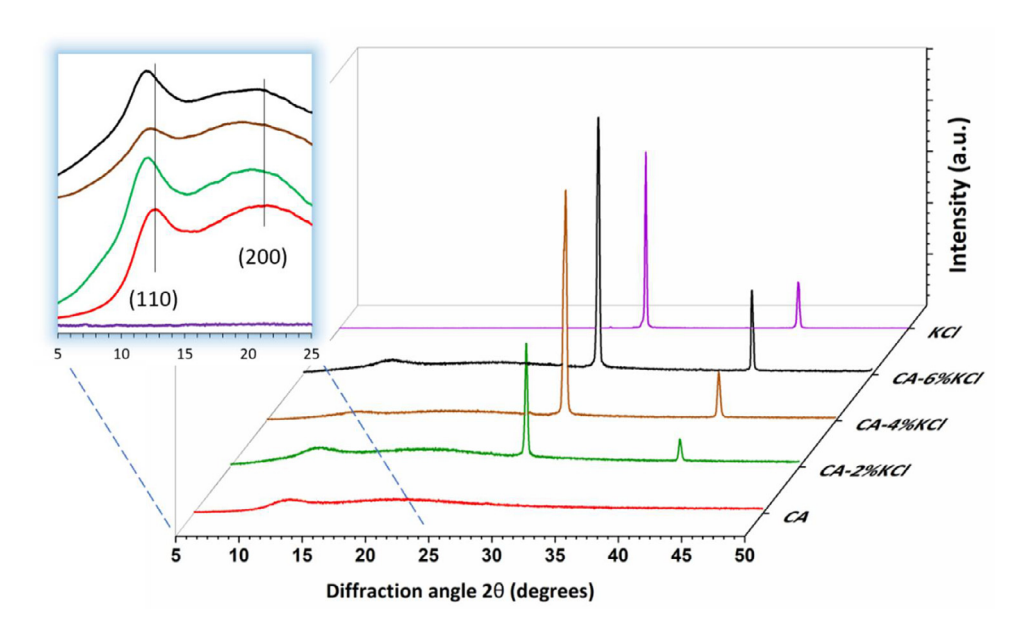


Fig. 6. XRD pattern of CA-KCl fiber mats. The patterns of KCl and CA were used as the reference. The pattern from 5 to 25° was smoothened using Savitzky-Golay filter (50-point first order) on Origin Plot. All the CA-KCL samples showed the four peaks corresponding to pure CA and KCl albeit with small shift, indicating presence of their native form post solution treatment.

planes [24]. These two peaks have been reported to vary from 8.7° to 15.7° and 17.2° to 22°, respectively, depending on the cellulose source [24,30,31,39]. Pure KCl also demonstrates two sharp peaks, at 29.2° and 41.3° [40]. The CA-KCl fiber mats exhibited all these four peaks but with a subtle shift in peak angle and intensity (Fig. 6), which could be attributed to the distribution of KCl in the CA matrix. Interestingly, no new diffraction peaks were noticed in the pattern suggesting the retention of CA structure within the crystalline region of CA-KCl mats along with the excess presence of KCl. However, the FTIR analysis indicated the interaction of K+ ions with the acetyl groups of cellulose, as discussed in Section 3.2. Based on XRD results, such interactions could be mostly in the amorphous region or have a smaller contribution to be able to be picked up by XRD as a new peak. Further research is warranted to decipher the optimum amount of K⁺ ions binding to the acetate groups. Overall, XRD data showed the maintenance of fiber morphology post solution treatment in these samples.

3.4. Tensile Response of CA vs. CA-KCl fiber Mats

Multiple tensile tests were performed for pure CA (control sample), pure-CA post dipping, and each type of RT air-dried CA-KCl fiber mats to understand the effect of KCl on mechanical properties. The number of samples was 10, 3, 9, 4, and 4 for pure CA, dipped CA, CA-2%KCl, CA-4%KCl, and CA-6%KCl. Fig. 7 shows a stress-strain graph where each plot is a representative data of each type of fiber mat having stiffness closest to the average plot.

For pure CA, the elastic modulus (up to 0.5 %strain) was 3.41 \pm 0.67 MPa and tensile strength was 0.14 \pm 0.02 MPa. For CA dipped in water, the elastic modulus (up to 0.5 %strain) was 11.55 \pm 4.15 MPa and tensile strength to 0.22 \pm 0.05 MPa. For CA-2%KCl, the elastic modulus (up to 0.1 %strain) was 23.326 \pm 8.72 MPa and tensile strength was 0.69 \pm 0.20 MPa. For CA-4%KCl, the elastic modulus (up to 0.2 %strain) was 127.92 \pm 44.56 MPa, and tensile strength was 1.10 \pm 0.14 MPa. For CA-6%KCl, the elastic modulus (up to 0.2 %strain) was 176.14 \pm 38.32 MPa, and tensile strength was 1.19 \pm 0.13 MPa. It is to be noted that the elastic moduli of each type of fiber mats are calculated until the strain at which the stress-strain behavior is linear. Hence, strain for modulus calculation varies across samples.

Pure CA-dipped in water exhibited 3.39 times increase in the elastic modulus and 1.62 times increase in tensile strength than pure CA. This change is mainly attributed to pore closure post dipping. CA-2%KCl

exhibited a 6.8 times increase in the elastic modulus and a 5 times increase in tensile strength. A significant difference (p-value < 0.05) in the mechanical property for pure CA was observed. These further increasing stiffness and strength beyond CA-dipped values showed the strengthening effect of KCl on CA fiber mats beyond pore closure. Subsequently, CA-4%KCl had a drastic increase in elastic modulus by 37.5 times and tensile strength by 8 times compared to pure CA. Lastly, CA-6%KCl fibers show a comparatively smaller rise in mechanical properties relative to CA-4%KCl with 51.7 times rise in elastic modulus and 8.62 times rise in tensile strength compared to pure CA. A very insignificant difference in elastic modulus (p-value = 0.25) and tensile strength (p-value = 0.14) compared to CA-4%KCl was observed.

The percentage deviation of properties relative to their respective mean values was also calculated to understand the variation in results between types of samples. The mechanical strength variation was highest in CA-2%KCl at \pm 30% from its mean. For all others, the variation was between 10 to 17%.

4. Discussion

The study revealed increased elastic modulus and tensile strength of electrospun CA fiber mat post KCl solution dipping. It is to be noted that the increase in mechanical properties of CA-KCl fiber mat compared to that of pure CA fiber mat dipped in water and air-dried further indicates the effect of KCl independent of pore removal due to solution dipping. Moreover, we kept the total time and other manufacturing parameters consistent across all samples to remove manufacturing variability in the electrospun mats. Other testing on the fibrous mat included SEM, FTIR, and XRD. SEM revealed some salt aggregation on the electrospun mat. FTIR study indicated chemical interaction between K⁺ and acetyl groups. XRD data revealed the maintenance of fiber morphology post solution. Together, the study showed the potential strengthening effect of electrospun CA fiber post KCl enrichment.

The expected mechanism behind the increase in mechanical properties can be explained via a combination of two effects: salt deposition observed in SEM, and the chemical interaction of potassium ions and acetyl groups found via FTIR. For CA-2% KCl, the salt deposition is small, reflected in a minimum change in its relative weight (Fig. 3) and SEM images (Fig. 4). Moreover, the limited salt deposits were distributed randomly on the fiber mat (Fig. 4), leading to a more distributed effect. Hence, the impact of salt deposition on mechanical properties is expected to be minimal compared to chemical interaction. The FTIR

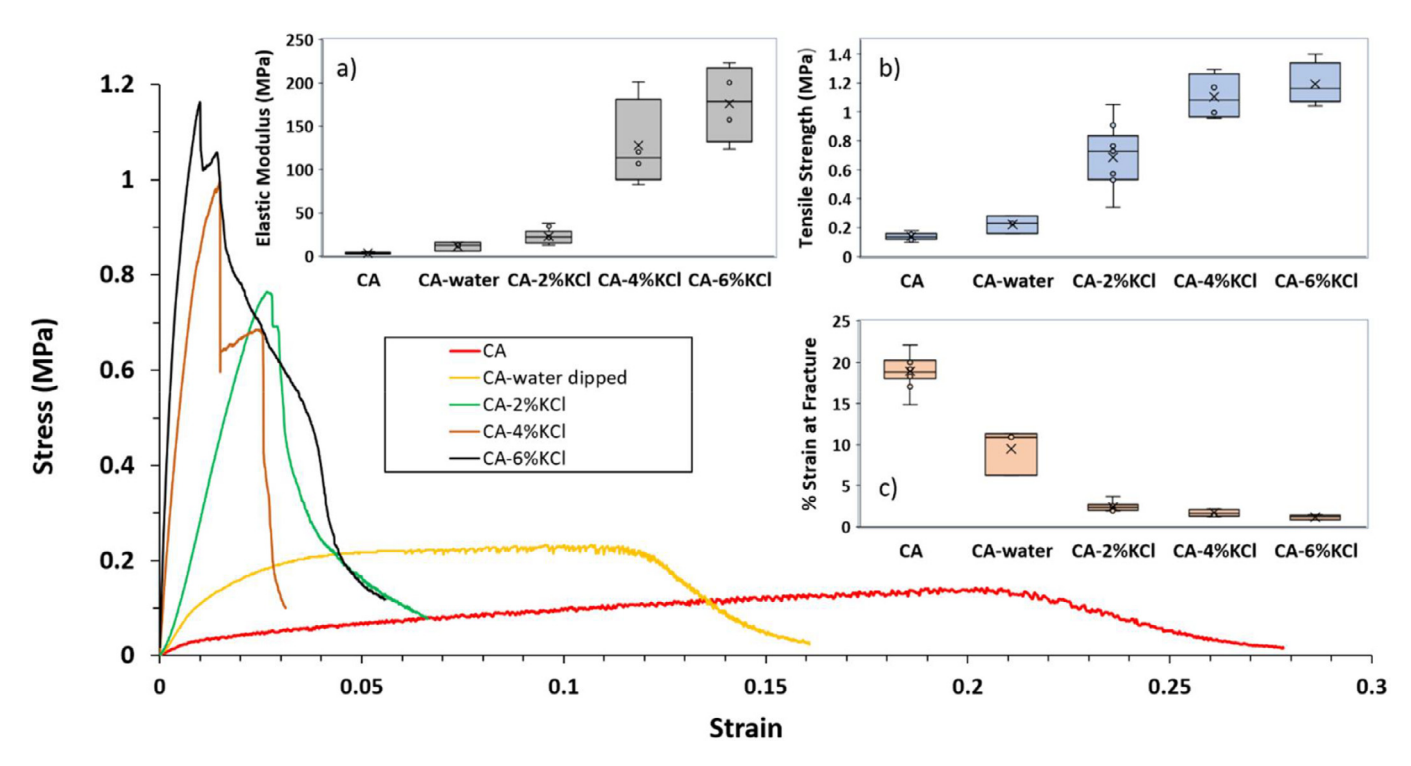


Fig. 7. Representative stress-strain plot of each type of fibers mats with its mechanical properties represented as box plots: a) Elastic modulus (in MPa) b) Tensile strength (in MPa) c) Percentage strain at fracture

analysis indicated the potential chemical interaction between the C-O bond in the acetyl group and positively charged K⁺ ions (Fig. 5). The pure CA fiber morphology did not change as a result of dipping as indicated by XRD (Fig. 6). The drastic increase in stiffness and strength observed for CA-2%KCl compared to pure CA and dipped-CA (Fig. 7) could thus be attributed primarily to chemical interactions.

For CA-4% KCl and CA-6%KCl, salt deposits were more prominent and uniformly distributed observed via an increase of relative weight (Fig. 3) and SEM data (Fig. 4). Notably, CA-4%KCl fiber mat had the highest increase in elastic modulus, indicating an increase in the number of electrostatic interactions between CA chains and K+ ions. For CA-6% KCl, there was no significant increase in the elastic modulus presumably due to saturation in chemical interactions between CA chains and K⁺ ions despite the rise of salt deposition. Together it indicates the higher impact from chemical interaction compared to increasing salt deposits on these mechanical properties of fiber mats. Secondary failure peaks were also observed for CA-KCl tensile response. The possibility of slippage of grips was ruled out due to the resurgence of stress after failure and the consistency of the phenomenon across different samples. A closer look at the failure locations (Fig. 8) of the testing samples revealed two failure locations: the first one is on the outer surface, and the second one is on the inner surface. Thus, it is inferred that the mechanical behavior of the CA fibers in the inner folds is different from the outer. The inside folds have lower salt penetration leading to lower salt deposit and/or chemical interaction. Hence, the first failure peak is attributed to the failure of the stiffer outer zone, and the second failure is attributed to the failure of inner folds.

The mechanical property of pure CA fiber mats, especially its tensile strength, seems to be on the lower end from values reported in other studies of electrospun CA fibers, as summarized in Table 2. It should be noted that the mechanical properties of the fiber mat are very much dependent on the fiber diameter, the density of the network, and the degree of alignment. A model predicted 3.5 and 8.5 times increase in the modulus with the change in fiber alignment from isotropic to moderately aligned and highly aligned, respectively [41]. Overall, the strength reported will be a function of testing parameters such as strain rate and

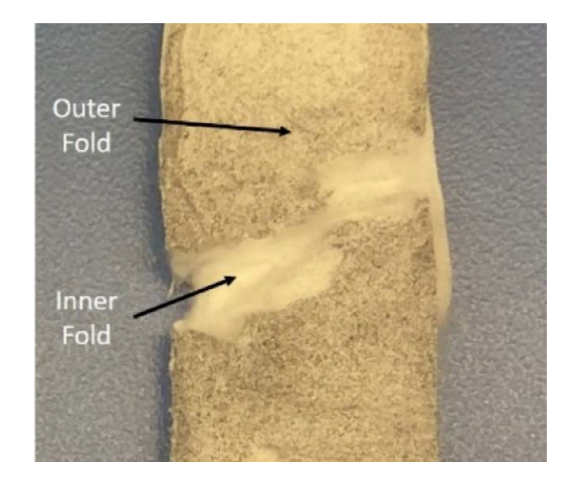


Fig. 8. Magnified view of the fracture zone of a CA-KCl fiber mat. The black dots are due to black sprays for better visibility of outer vs. inner fold.

fiber mat morphology. Fiber mat morphology in turn will depend on manufacturing parameters.

To investigate some of these aspects and compare them with reported values, fiber diameter, and pore-size analysis were carried out on pure CA SEM image (Fig. 2a) using DiameterJ, an extension to ImageJ/FIJI [42,43]. The result of the analysis is shown in Fig. 9. The average cumulative diameter was found to be 0.827 \pm 0.4057 μm . The median value of the pore size was found out to be 1.04 μm . In comparison, the fiber diameter reported in Table 2 varied from 200 nm to 13.3 μm , with a lower tensile strength value of 1.2 MPa reported for diameters in the range of 0.2 to 1 μm . The fiber diameter and results reported here fall closer to the lower values reported for larger diameter fibers. However, a one-to-one comparison is not possible due to the variation of strain rate of testing.

 Table 2

 Different parameters used in electrospinning and tensile test samples of various modifications of CA fibers and the corresponding mechanical properties.

No	Electrospinning parameters				Strain	Fiber	Mechanical Property (pure CA)			Ref		
	M _W 1000	Wt%	Voltage (kV)	Distance (cm)	Flow Rate (mL/h)	Solvent	Rate (mm/min)	Diameter (nm)	$\sigma_{ m T}$ MPa	E MPa	ε _f (%)	
1	29	**	25	15	4	Acetone:DMF:TFE (3:1:1)	10	200-1000	1.2*	1*	15*	[28]
2	50	**	26-28	15	0.07-0.14	Acetone:DMF (3:2)	_**	515 ± 45	45*	100	44*	[30]
3	30	19	12	15	**	Acetone:DMF (3:2)	5	580 ± 200	*ok	247	**	[24]
4	50	15	27	15	0.13	Acetone:DMF (3:2)	2	300 ± 25	49	400	27*	[31]
5	30	**	20	10	6-18	TFA:acetic acid (7:3)	10	331 ± 118	2.16*	9*	4.5*	[29]
6	50	**	25	25	90	Ethyl Acetate	25	5×10^{3}	3.8	34.7	27	[32]
7	29	15	15	15	6	Acetone	0.2	$(13.3 \pm 3.5) \times 10^3$	NOR	7.3 ± 1.8	13	[41]
8	50	12	20	20	0.2	Acetone:DMF (2:1)	5	**	2-3	**	**	[44]
9	30	15	15	18	12	Acetone	2	827 ± 405.7	0.14 ± 0.4	3.41 ± 0.7	18.9 ± 1.3	This work

^{*} data approximated from stress-strain plots,

^{**} values not reported

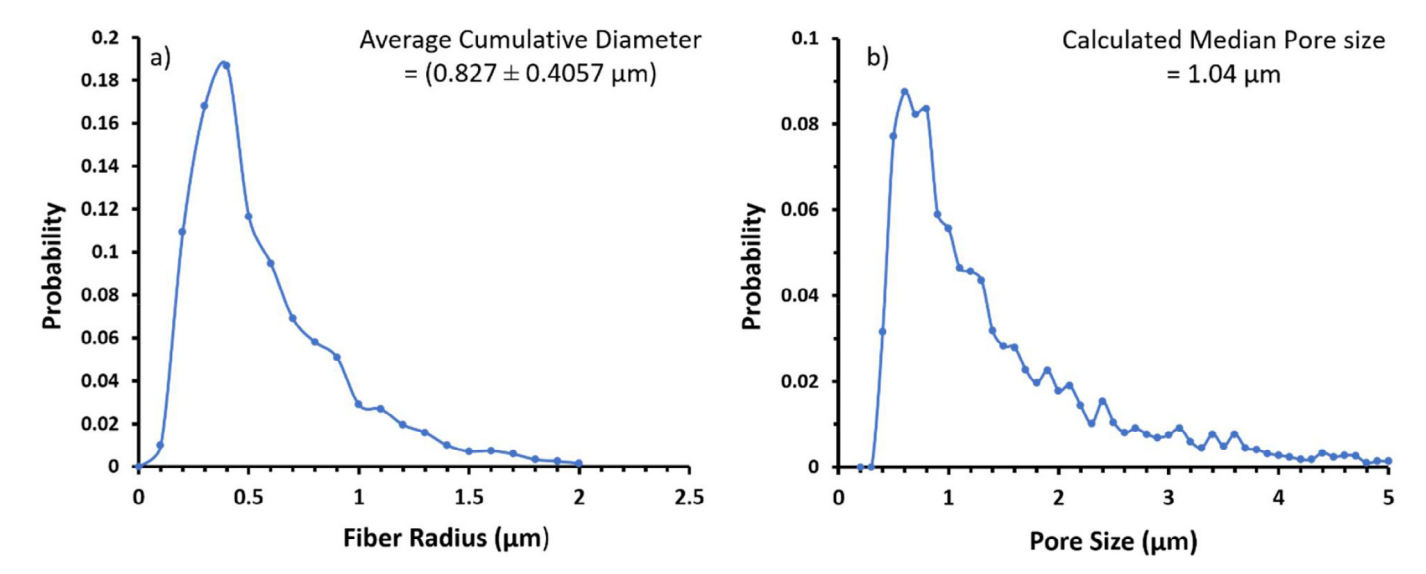


Fig. 9. Calculation of morphology of pure CA (Fig. 2a) electrospun fiber mat using ImageJ a) Fiber radius distribution b) Pore Size distribution calculated from the minor pore axis length.

Additionally, significant variations in electrospinning parameters also exist among studies. We used CA with molecular weight 30,000 g/mol, while studies reported values from 29,000 to 50,000. The concentration and type of solution is another factor influencing the outcome. The tensile modulus was reported to increase from 3.5 to 12.4 MPa as the CA concentration in acetone rose from 10 to 17.5 % [41]. Finally, the different or unreported strain rate of the tensile tests also makes comparisons difficult, as stated earlier. Taken together, these mismatches in fiber diameter, distribution, molecular weight, and solvent concentration are expected to be the underlying reasons for observed significant property variation among sources. Moving forward, a way of validation and reporting fiber mat strength could be calculating the mechanical property of a single CA fiber, to compare against theoretical values. This approach will be taken in future studies such as the sonication-induced scission for fiber strength calculation [44].

4.1. Future Work for Bone Tissue Engineering Applications

In this work, the elastic modulus of CA-KCl fiber mats has been significantly enhanced to 23, 128, and 176 MPa, and a modest increase in tensile strength to 0.7, 1.1, 1.2 MPa by treating with 2, 4, and 6 % KCl, respectively. Hence, the stiffness of the fiber mat can be tuned according to the mechanical property of the tissue required. For comparison, the elastic modulus of trabecular bone has been reported within a range of 10 to 20,000 MPa depending on porosity and density [45–49]. Nonetheless, the two-dimensional shape of electrospun fiber mat can

be a hindrance to its potential substitute for large bone defects. Studies have shown a significant deviation of results in cell activities from 2D to 3D matrix in terms of cell proliferation, differentiation, and mechanotransduction [50]. The pore size of a minimum of 100 μ m is another requirement for osteogenesis, with and pores sizes larger than 350 μ m for vascularization [51]. Here, a much finer pore of 1.04 μ m median size was reported. Lyophilization of cellulose acetate gel has been proven to control the porous structure to obtain the desired 3D morphology with micro and macro pores.

The compressive properties of the scaffold generated are equally crucial for efficient cell proliferation and should be able to withstand a physiological strain of 2500 $\mu\epsilon$ [52]. Hence, tuning the mechanical properties of the CA fibrous scaffold by lyophilization and K+ treatment, and a suitable choice of the matrix for compressive strength is one promising approach to achieve the desired 3D bone tissue microenvironment. Finally, cell viability studies are needed to prove the biocompatibility and tissue regeneration properties of the scaffold. These aspects are the focus of our continued work.

5. Conclusions

Electrospun CA fibers have been used widely in tissue engineering applications due to their optimum morphology and resorbability. However, pure CA fibers have inadequate mechanical properties, especially for bone tissue engineering. The proposed methodology of treating potassium chloride to cellulose acetate seems to be effective in

enhancing the tensile mechanical properties along with its added benefits in bone cell proliferation, making it a promising biomaterial for bone tissue engineering. The mechanical properties such as tensile strength and elastic modulus can be increased 7 times from 0.2 MPa to 1.4 MPa and around 50 times from 4 MPa to 200 MPa respectively by increasing the KCl concentration. The interaction between K⁺ and acetyl group of CA fiber mat was identified to be the mechanism behind increased behavior in addition to the salt deposition on the fiber mat and removal of pores while dipping in the solution. The presence of potassium ions yields added benefits desirable for bone tissue engineering.

The study thus shows the implications of enhanced CA fiber mat in the presence of KCl. These results can have a profound influence on bone tissue engineering applications. Thus, the proposed research paves the way for future studies of enhanced CA-KCl 3D structures via lyophilization as cell-growth and bone-tissue microenvironment.

Declaration of Competing interest

The authors declare that they have no known competing financial interests or personal relationships that could have appeared to influence the work reported in this paper.

Acknowledgments

Support is Jerome J. Lohr College of Engineering Graduate Assistantship to RS, SunGrant (SA1800557) to AP, and USDA National Institute for Food and Agriculture (HATCH project SD00H648-18) to SJ. Review comments by Dr. Travis Burgers are much appreciated.

References

- M.F. Ashby, L.J. Gibson, U. Wegst, R. Olive, The mechanical properties of natural materials. i. material property charts, Proceed.: Math. Phys. Sci. 450 (1995) 123–140 https://www.jstor.org/stable/52662. (accessed April 27, 2020).
- [2] V.A. Bazhenov, Piezoelectric properties of wood, Consultants Bureau, New York, 1961.
- [3] D. Klemm, B. Heublein, H. Fink, A. Bohn, Cellulose: fascinating biopolymer and sustainable raw material, Angew. Chem. Int. Ed. 44 (2005) 3358–3393, doi:10.1002/ANIF.200460587.
- [4] N. Lin, A. Dufresne, Nanocellulose in biomedicine: current status and future prospect, Eur. Polym. J. 59 (2014) 302–325, doi:10.1016/j.eurpolymj.2014.07.025.
- [5] H. Du, W. Liu, M. Zhang, C. Si, X. Zhang, B. Li, Cellulose nanocrystals and cellulose nanofibrils based hydrogels for biomedical applications, Carbohydr. Polym. 209 (2019) 130–144, doi:10.1016/j.carbpol.2019.01.020.
- [6] S.S. Athukoralalage, R. Balu, N.K. Dutta, N. Roy Choudhury, 3D bioprinted Nanocellulose-based hydrogels for tissue engineering applications: a brief review, Polymers 11 (2019) 898, doi:10.3390/polym11050898.
- [7] M. Kemell, V. Pore, M. Ritala, M. Leskelä, M. Lindén, Atomic layer deposition in nanometer-level replication of cellulosic substances and preparation of photocatalytic TiO2/Cellulose composites, J. Am. Chem. Soc. 127 (2005) 14178–14179, doi:10.1021/ja0532887.
- [8] T. Nishino, N. Arimoto, All-Cellulose Composite Prepared by Selective Dissolving of Fiber Surface, Biomacromolecules 8 (2007) 2712–2716, doi:10.1021/bm0703416.
- [9] H. Wang, L. Kong, G.R. Ziegler, Fabrication of starch Nanocellulose composite fibers by electrospinning, Food Hydrocoll. 90 (2019) 90–98, doi:10.1016/j.foodhyd.2018.11.047.
- [10] J. Kim, S. Yun, Z. Ounaies, Discovery of Cellulose as a Smart Material, Macro-molecules 39 (2006) 4202–4206, doi:10.1021/ma060261e.
- [11] Q. Xu, C. Chen, K. Rosswurm, T. Yao, S. Janaswamy, A facile route to prepare cellulose-based films, Carbohydr. Polym. 149 (2016) 274–281, doi:10.1016/j.carbpol.2016.04.114.
- [12] P. Gouma, R. Xue, C.P. Goldbeck, P. Perrotta, C. Balázsi, Nano-hydroxyapatite -Cellulose acetate composites for growing of bone cells, Mater. Sci. Eng. C 32 (2012) 607–612. doi:10.1016/j.msec.2011.12.019.
- [13] D. Atila, D. Keskin, A. Tezcaner, Crosslinked pullulan/cellulose acetate fibrous scaffolds for bone tissue engineering, Mater. Sci. Eng. C 69 (2016) 1103–1115, doi:10.1016/j.msec.2016.08.015.
- [14] L. Wang, H. Lv, L. Liu, Q. Zhang, P. Nakielski, Y. Si, J. Cao, X. Li, F. Pierini, J. Yu, B. Ding, Electrospun nanofiber-reinforced three-dimensional chitosan matrices: Architectural, mechanical and biological properties, J. Colloid Interface Sci. 565 (2020) 416–425, doi:10.1016/j.jcis.2020.01.016.
- [15] S. Mayer-Wagner, T.S. Schiergens, B. Sievers, D. Docheva, M. Schieker, O.B. Betz, V. Jansson, P.E. Müller, Membrane-based cultures generate scaffold-free neocartilage in vitro: Influence of growth factors, Tissue Eng. - Part A 16 (2010) 513–521, doi:10.1089/ten.tea.2009.0326.
- [16] D. Atila, D. Keskin, A. Tezcaner, Cellulose acetate based 3-dimensional electrospun scaffolds for skin tissue engineering applications, Carbohydr. Polym. 133 (2015) 251–261, doi:10.1016/j.carbpol.2015.06.109.

[17] S. Farzamfar, M. Naseri-Nosar, A. Vaez, F. Esmaeilpour, A. Ehterami, H. Sahrapeyma, H. Samadian, A.A. Hamidieh, S. Ghorbani, A. Goodarzi, A. Azimi, M. Salehi, Neural tissue regeneration by a gabapentin-loaded cellulose acetate/gelatin wet-electrospun scaffold, Cellulose 25 (2018) 1229–1238, doi:10.1007/s10570-017-1632-z.

- [18] A.P. Kishan, E.M. Cosgriff-Hernandez, Recent advancements in electrospinning design for tissue engineering applications: A review, J. Biomed. Mater. Res. - Part A 105 (2017) 2892–2905. doi:10.1002/jbm.a.36124.
- [19] M. Zhang, W. Ma, J. Cui, S. Wu, J. Han, Y. Zou, C. Huang, Hydrothermal synthesized UV-resistance and transparent coating composited superoloephilic electrospun membrane for high efficiency oily wastewater treatment, J. Hazard. Mater. 383 (2020) 121152, doi:10.1016/j.jhazmat.2019.121152.
- [20] M. Zhu, D. Hua, H. Pan, F. Wang, B. Manshian, S.J. Soenen, R. Xiong, C. Huang, Green electrospun and crosslinked poly(vinyl alcohol)/poly(acrylic acid) composite membranes for antibacterial effective air filtration, J. Colloid Interface Sci. 511 (2018) 411–423, doi:10.1016/j.jcis.2017.09.101.
- [21] D. Lv, R. Wang, G. Tang, Z. Mou, J. Lei, J. Han, S. De Smedt, R. Xiong, C. Huang, Ecofriendly Electrospun Membranes Loaded with Visible-Light-Responding Nanoparticles for Multifunctional Usages: Highly Efficient Air Filtration, Dye Scavenging, and Bactericidal Activity, ACS Appl. Mater. Interfaces 11 (2019) 12880–12889, doi:10.1021/acsami.9b01508.
- [22] R. Al-Attabi, Y. Morsi, W. Kujawski, L. Kong, J.A. Schütz, L.F. Dumée, Wrinkled silica doped electrospun nano-fiber membranes with engineered roughness for advanced aerosol air filtration, Sep. Purif. Technol. 215 (2019) 500–507, doi:10.1016/j.seppur.2019.01.049.
- [23] S. Chattopadhyay, T.A. Hatton, G.C. Rutledge, Aerosol filtration using electrospun cellulose acetate fibers, J. Mater. Sci. 51 (2015) 204–217, doi:10.1007/s10853-015-9286-4.
- [24] M. Gopiraman, K. Fujimori, K. Zeeshan, B.S. Kim, I.S. Kim, Structural and mechanical properties of cellulose acetate/graphene hybrid nanofibers: spectroscopic investigations, Express Polym. Lett. 7 (2013) 554–563, doi:10.3144/expresspolymlett.2013.52.
- [25] A. Haider, S. Haider, I.K. Kang, A comprehensive review summarizing the effect of electrospinning parameters and potential applications of nanofibers in biomedical and biotechnology, Arabian J. Chem. 11 (2018) 1165–1188, doi:10.1016/j.arabjc.2015.11.015.
- [26] S. Majumder, M.A. Matin, A. Sharif, M.T. Arafat, Understanding solubility, spinnability and electrospinning behaviour of cellulose acetate using different solvent systems, Bull. Mater. Sci. 42 (2019) 1–9, doi:10.1007/s12034-019-1857-6.
- [27] H. Liu, Y. Lo Hsieh, Ultrafine fibrous cellulose membranes from electrospinning of cellulose acetate, J. Polym. Sci. Part B Polym. Phys. 40 (2002) 2119–2129, doi:10.1002/polb.10261.
- [28] Z. Ma, M. Kotaki, S. Ramakrishna, Electrospun cellulose nanofiber as affinity membrane, J. Membr. Sci. 265 (2005) 115–123, doi:10.1016/j.memsci.2005.04.044.
- [29] D.N. Phan, H. Lee, B. Huang, Y. Mukai, I.S. Kim, Fabrication of electrospun chitosan/cellulose nanofibers having adsorption property with enhanced mechanical property, Cellulose 26 (2019) 1781–1793, doi:10.1007/s10570-018-2169-5.
- [30] A. Salama, A. Mohamed, N.M. Aboamera, T. Osman, A. Khattab, Characterization and mechanical properties of cellulose acetate/carbon nanotube composite nanofibers, Adv. Polym. Technol. 37 (2018) 2446–2451, doi:10.1002/adv.21919.
- [31] N.M. Aboamera, A. Mohamed, A. Salama, A. Khattab, Characterization and mechanical properties of electrospun cellulose acetate/graphene oxide composite nanofibers, Mech. Adv. Mater. Struct. 26 (2019) 765–769, doi:10.1080/15376494.2017.1410914.
- [32] K.I. Lukanina, T.E. Grigoriev, S.V. Krasheninnikov, V.G. Mamagulashvilli, R.A. Kamyshinsky, S.N. Chvalun, Multi-hierarchical tissue-engineering ECM-like scaffolds based on cellulose acetate with collagen and chitosan fillers, Carbohydr. Polym. 191 (2018) 119–126, doi:10.1016/j.carbpol.2018.02.061.
- [33] H. Ishikawa, S. Tadano, Mechanical and optical characterization of cellulose acetate, Exp. Mech. 28 (1988) 221–225, doi:10.1007/BF02329014.
- [34] C.Y. Zheng, S.J. Li, X.J. Tao, Y.L. Hao, R. Yang, L. Zhang, Calcium phosphate coating of Ti-Nb-Zr-Sn titanium alloy, Mater. Sci. Eng. C 27 (2007) 824–831, doi:10.1016/j.msec.2006.09.021.
- [35] S.N. Nayab, F.H. Jones, I. Olsen, Human alveolar bone cell adhesion and growth on ion-implanted titanium, J. Biomed. Mater. Res. - Part A 69 (2004) 651–657, doi:10.1002/jbm.a.30032.
- [36] Q. Xu, C. Chen, K. Rosswurm, T. Yao, S. Janaswamy, A facile route to prepare cellulose-based films, Carbohydr. Polym. 149 (2016) 274–281, doi:10.1016/j.carbpol.2016.04.114.
- [37] E. Goldstein, J. Newbury, E. Dale, Patrick Echlin, David C. Joy, Alton D. Romig Jr., Charles E. Lyman, Charles Fiori, Lifshin, Scanning Electron Microscopy and X-Ray Microanalysis: A Text for Biologists, Materials Scientists, and Geologists, 2nd ed., Springer US, New York and London, 1992.
- [38] P. Fei, L. Liao, B. Cheng, J. Song, Quantitative analysis of cellulose acetate with a high degree of substitution by FTIR and its application, Anal. Methods 9 (2017) 6194–6201. doi:10.1039/c7av02165h.
- [39] E. Huda, Khairan Rahmi, Preparation and characterization of cellulose acetate from cotton, IOP Conf. Ser.: Earth Environ. Sci. (2019) 364, doi:10.1088/1755-1315/364/1/012021.
- [40] M. Agarwal, S.K. Garg, K. Asokan, D. Kanjilal, P. Kumar, Facile synthesis of KCI:Sm3+ nanophosphor as a new OSL dosimetric material achieved through charge transfer between the defect states, RSC Adv. 7 (2017) 13836–13845, doi:10.1039/cfra25237k.
- [41] T. Stylianopoulos, M. Kokonou, S. Michael, A. Tryfonos, C. Rebholz, A.D. Odysseos, C. Doumanidis, Tensile mechanical properties and hydraulic permeabilities of electrospun cellulose acetate fiber meshes, J. Biomed. Mater. Res. Part B: Appl. Biomater. 100B (2012) 2222–2230, doi:10.1002/jbm.b.32791.

[42] J. Schindelin, I. Arganda-Carreras, E. Frise, V. Kaynig, M. Longair, T. Pietzsch, S. Preibisch, C. Rueden, S. Saalfeld, B. Schmid, J.Y. Tinevez, D.J. White, V. Hartenstein, K. Eliceiri, P. Tomancak, A. Cardona, Fiji: An open-source platform for biological-image analysis, Nat. Methods 9 (2012) 676–682, doi:10.1038/nmeth.2019.

- [43] N.A. Hotaling, K. Bharti, H. Kriel, C.G. Simon, DiameterJ: A validated open source nanofiber diameter measurement tool, Biomaterials 61 (2015) 327–338, doi:10.1016/j.biomaterials.2015.05.015.
- [44] J. Avô, S.N. Fernandes, M.H. Godinho, Revealing the hierarchical mechanical strength of single cellulose acetate electrospun filaments through ultrasonic breakage, Macromol. Rapid Commun. 36 (2015) 1166–1170, doi:10.1002/marc.201500087.
- [45] S.A. Goldstein, The mechanical properties of trabecular bone: Dependence on anatomic location and function, J. Biomech. 20 (1987) 1055–1061, doi:10.1016/0021-9290(87)90023-6.
- [46] R. Oftadeh, M. Perez-Viloria, J.C. Villa-Camacho, A. Vaziri, A. Nazarian, Biomechanics and mechanobiology of trabecular bone: a review, J. Biomech. Eng. (2015) 137, doi:10.1115/1.4029176.

- [47] M. Pawlikowski, K. Skalski, J. Bańczerowski, A. Makuch, K. Jankowski, Stress-strain characteristic of human trabecular bone based on depth sensing indentation measurements, Biocybern. Biomed. Eng. 37 (2017) 272–280, doi:10.1016/j.bbe.2017.01.002.
- [48] E.F. Morgan, G.U. Unnikrisnan, A.I. Hussein, Bone Mechanical Properties in Healthy and Diseased States, Annu. Rev. Biomed. Eng. 20 (2018) 119–143, doi:10.1146/annurev-bioeng-062117-121139.
- [49] E.F. Morgan, H.H. Bayraktar, T.M. Keaveny, Trabecular bone modulus-density relationships depend on anatomic site, J. Biomech. 36 (2003) 897–904, doi:10.1016/S0021-9290(03)00071-X.
- [50] K. Duval, H. Grover, L.H. Han, Y. Mou, A.F. Pegoraro, J. Fredberg, Z. Chen, Modeling physiological events in 2D vs. 3D cell culture, Physiology 32 (2017) 266–277, doi:10.1152/physiol.00036.2016.
- [51] O. Petrauskaite, G. Juodzbalys, P. Viskelis, J. Liesiene, Control of the porous structure of cellulose-based tissue engineering scaffolds by means of lyophilization, Cellul. Chem. Technol. 50 (2016) 23–30.
- [52] Y. Yan, Y. Gong, Y. Guo, Q. Lv, C. Guo, Y. Zhuang, Y. Zhang, R. Li, Mechanical Strain Regulates Osteoblast Proliferation through Integrin-Mediated, ERK Act. 7 (2012) 1– 14, doi:10.1371/journal.pone.0035709.